Effects of electron-hole separation on the photoconductivity of individual metal oxide nanowires

J D Prades[*,1], F Hernandez-Ramirez[*,1,2], R Jimenez-Diaz[1], M Manzanares[1], T Andreu[1], A Cirera[1], A Romano-Rodriguez[1] and J R Morante[1]
[1]EME/XaRMAE/IN[2]UB, Departament d'Electrònica, Universitat de Barcelona, C/ Martí i Franquès 1, E-08028 Barcelona, Spain
[2] Electronic Nanosystems S. L., Barcelona, Spain

E-mail: dprades@el.ub.es, fhernandez@gmail.com

Abstract. Responses of individual ZnO nanowires to UV light demonstrate that the Persistent PhotoConductivity (PPC) state is directly related to the electron-hole separation near the surface. Our results demonstrate that the electrical transport in these nanomaterials is influenced by the surface in two different ways. On the one hand, the effective mobility and the density of free carriers are determined by recombination mechanisms assisted by the oxidizing molecules in air. This phenomenon can also be blocked by surface passivation. On the other hand, the surface built-in potential separates the photogenerated electron-hole pairs and accumulates holes at the surface. After illumination, the charge separation makes difficult the electron-hole recombination and originates PPC. This effect is quickly reverted after increasing either the probing current (self-heating by Joule dissipation) or the oxygen content in air (favouring the surface recombination mechanisms). The here-presented model for PPC in individual nanowires illustrates the intrinsic potential of metal oxide nanowires to develop optoelectronic devices or optochemical sensors with better and new performances.

1. Introduction

Methods for synthesis of nanomaterials have undergone a huge improvement in the last years [1,2], providing researchers with nanowires with high surface-to-volume ratio and excellent crystalline properties [3,4]. Their electrical characterization is a direct way to gain a deep comprehension of some of the phenomena typical of the nanoscale, which are originated due to the overexposure of the bulk of nanomaterials to surface effects [5,6,7]. To date, the large majority of works have focused on the study of nanowire bundles [8], but uncontrolled parasitic effects between nanowires has made difficult obtaining any conclusive result [9]. The constant improvement of nanofabrication techniques is slowly changing this situation, enabling the appearance of many works dealing with individual nanowires, and whose electrical characterization is extremely helpful to evaluate transport phenomena in single-crystal structures [10].

Among nanowires, metal-oxide ones are excellent candidates to evaluate the influence of surface effects on the bulk properties of nanomaterials, since they are highly reactive to their surrounding atmosphere [11]. This property has attracted an increasing interest to integrate them as building blocks of new nanodevices, like gas sensors or optoelectronic devices [6,7]. Zinc oxide (ZnO) nanowires are versatile metal-oxide nanomaterials which have been successfully tested in different fields [12], like chemical [3] and biological sensing [13], optoelectronics [6,7], energy harvesting [14], and ultraviolet (UV) photodetection [15-19]. In this last case, they even exhibit higher photoconductive gains [18,19] than equivalent devices based on thin film technologies [20].

[*] Authors to whom any correspondence should be addressed.

The effects of UV light on ZnO are more complex than a simple band-to-band photoresponse [15-19], since it often induces a persistent increase of the electrical conductivity which lasts for a long time after the exposure to UV [21-30] and requires a post-treatment of the sample to recover the initial value. The origin of this Persistent PhotoConductivity (PPC) phenomenon is still controversial. On the one hand, some authors relate PPC to either intrinsic or extrinsic point defects which exhibit metastable charge states [21-23]. On the other hand, others claim that the origin is the electron-hole separation related to the surface properties of metal oxides [24-27,29,30]. Thus, a widely accepted description has not been presented yet [23].

In this paper, the strong influence of surface effects on the transport phenomena of nanomaterials has been used to evaluate the PPC effect in individual ZnO nanowires and demonstrate its surface origin. Unlike previous works, here, the use of a single nanowire has allowed to exclude other influences and experimentally simplify the analysis. We have studied the influence of the surface recombination mechanisms on PPC via the effective mobility and the density of free carriers. Moreover, the PPC recovery at different working conditions (probing currents and atmospheres) has also been studied in detail. Based on these results, a model for PPC in a single nanowire is presented, and different strategies to minimize or even block the PPC in ZnO are outlined, enabling the design of nanowire-based photodetectors free of this undesirable effect.

2. Experimental details

ZnO nanowires [3,31] (see supporting information) were dispersed in propylenglycol and deposited onto an insulating SiO_2 chip with pre-patterned Au / Ti / Ni microelectrodes. Then, some of them were electrically contacted to the microelectrodes in 4-probe configuration with a FEI Dual-Beam Strata 235 Focused Ion Beam (FIB) equipped with a metalorganic precursor to deposit Pt strips (figure 1) [32], following a methodology designed to minimize structural modification during the fabrication process [9]. The electrical response of the final devices was evaluated inside a home-made chamber specially designed to illuminate the sample at the same time than different atmospheres were applied with the help of four gas mass-flow systems. The light power impinging on this sample (λ = 340 ± 10 nm) was estimated with a photodiode located beside it [33]. A home-made electronic circuit designed to guarantee that low current levels I_m (from 0.1 nA to 250 nA) were applied during the experiments was used [34], and parasitic effects of the metal-nanowire contacts were avoided performing 4-probing DC measurements [10] (see supporting information). Fifteen of these devices exhibited stable characteristics without any noticeable degradation after three weeks of continuous operation. All the experiments were performed in either synthetic air (SA) or nitrogen (N_2). Finally, some of them were passivated with a 470 nm thick PMMA layer deposited by spin coating. This layer was UV transparent and electrically insulating (see supporting information).

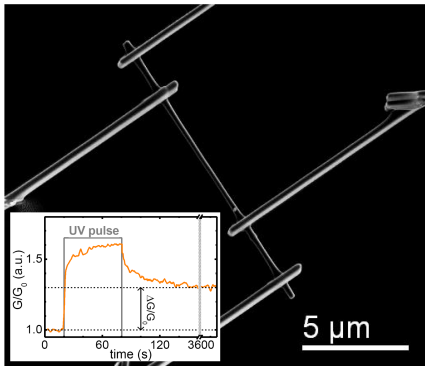

Figure 1. ZnO nanowire of length L_{NW} = 13 µm and radius r_{NW} ~ 95 nm electrically contacted with FIB nanolithography techniques. (Inset) Evidence of PPC in these nanowires: the conductance baseline was not fully recovered after switching off the light.

3. Experimental Results and Discussion

3.1 Evidence of PPC in individual ZnO nanowires

Non illuminated ZnO nanowires (length L_{NW} = 13 µm and radius r_{NW} ~ 95 nm) in oxygen rich atmospheres exhibited conductance values of $G_{0(SA)}$ = 59 ± 6 nS, which are in agreement with reported data [15-19] (see supporting information). No significant photoresponse was observed with impinging photons with energies hν below the bandgap of ZnO (E_{gap} = 3.37eV [35]) (see supporting information). On the contrary, photons with higher energies lead to an important increase of the electrical conductance of nanowires. This result confirms that photoconduction in ZnO nanowires is mainly originated by band-to-band electron-hole pair generation in their bulk. Dynamic measurements showed that the conductance baseline was not fully recovered after switching off the light, demonstrating the existence of PPC in these nanomaterials (inset in figure 1).

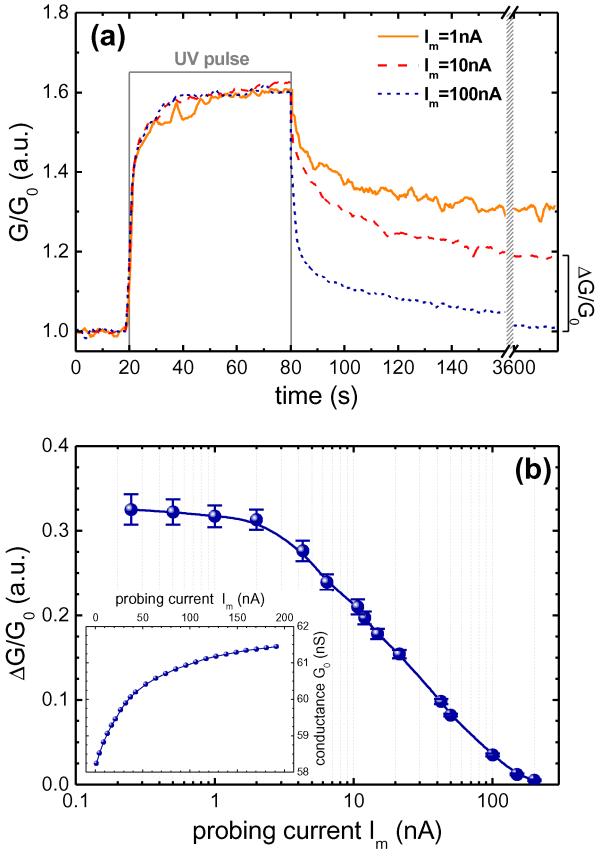

Figure 2. (a) Relative conductance change (G/G_0) of a ZnO nanowire under illumination (60 s UV pulse, photon flux Φ_{ph} = $3.3 \cdot 10^{18}$ $m^{-2}s^{-1}$, wavelength λ = 340 ± 10nm) acquired at three different current levels (I_m) in synthetic air. Axis break shows the conductance one hour later. (b) Dependence of the PPC with the probing current I_m in synthetic air. The magnitude of the PPC ($\Delta G/G_0$) was determined as described in the text. PPC values and error bars shown in the figure are the mean and the standard deviation of the results obtained with ten different samples. The dependence of the conductance in dark (G_0) with the probing current is shown in the inset. Conductance rise demonstrates the self-heating of the nanowires during the measurement, in accordance with the semiconductor character of ZnO.

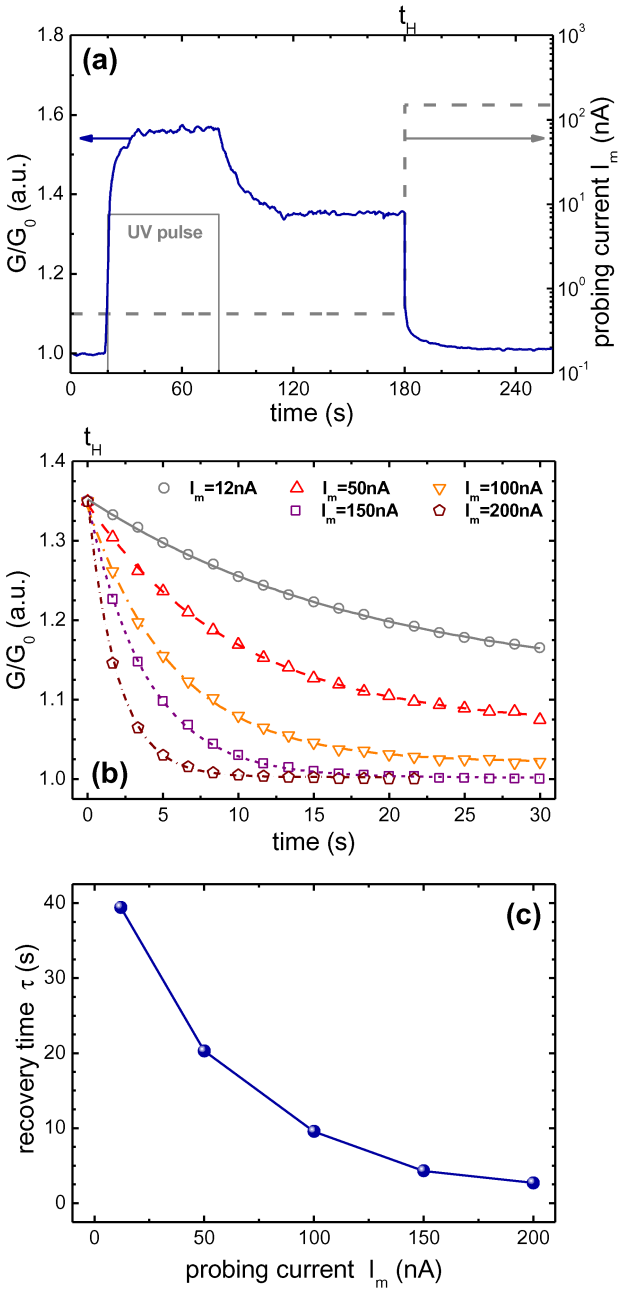

Figure 3. Recovery of the PPC stimulated by high probing current values. (a) G/G_0 record. A 60s UV pulse was applied to a ZnO nanowire in low current conditions (I_m = 0.5nA). After the stabilization of the PPC (at t_H), the conductance recovery was stimulated by increasing the probing current (I_m = 150nA). (b) Analysis of the recovery transients for different I_m. Experimental data points fit to exponential decay laws (lines) to estimate the recovery time constants τ. (c) PPC recovery time constant τ as function of the probing current I_m.

3.2 Influence of the probing current on PPC

It was experimentally found that the intensity of PPC is directly related to the probing current (I_m) applied to the nanowires (figure 2). The recovery of the conductance G of a ZnO nanowire after a 60 second UV pulse at different I_m is shown in figure 2a. Here, the relative persistence of the conductance was defined as,

$$\frac{\Delta G}{G_0} = \frac{G_{1h} - G_0}{G_0} \quad (1)$$

where G_0 was the initial value in darkness and G_{1h} one hour after the pulse.
The PPC effect fully disappeared one hour after illuminating the sample with $I_m > 100$ nA. On the contrary, PPC did not vanish with lower I_m, reaching a maximum with $I_m < 1$ nA (figure 2b). These two different behaviours are an indirect proof of the well-known dependence on PPC with temperature [21,25,26,36], since nanodevices reach high temperatures due to the dissipated electrical power when they come into operation. To validate this assumption, the recovery of G in a ZnO nanowire showing PPC was stimulated with a sudden increase of I_m from 0.5 nA to 150 nA (figure 3a). Transient responses in good correspondence with exponential decays were found in all the experiments (figure 3b). The higher the probing current I_m was applied to the nanodevices, the faster the recovery time was observed (figure 3c). Equivalent responses were monitored in SA and N_2. Thus, the modulation of I_m is proposed as a simple and fast methodology to control PPC, despite it does not shed light on the origin of PPC in ZnO. It goes without saying that an accurate estimation of the temperature reached by the nanowire due to Joule self-heating would provide valuable information about the activation energies of the states related to PPC, but this point remains as a complex experimental issue [37].

3.3 On the origin of PPC in ZnO nanowires

There are two opposite models which describe PPC in ZnO. The first one claims that this phenomenon is related to metastable bulk defects located between their shallow and deep energy levels [21-23]. According to this assumption, oxygen vacancies can be excited to a metastable charged state after a structural relaxation. In these states, the recapture of electrons is prevented by a thermally activated barrier [21]. The second one upholds that PPC is a pure surface effect related to the capture of electrons by surface states [26,27,29], which arise with the generation of oxygen vacancies by UV light [24,26,30]. This process is also reverted by temperature-assisted adsorption of oxygen species [26-28]. In these two theoretical approaches, if electron-hole pairs are spatially separated, their recombination rate is significantly reduced, giving rise to PPC.

3.3.a Evaluation of surface effects in PPC

To clarify the origin of PPC, individual ZnO nanowires were used to take advantage of the overexposure of their bulk to surface effects. I_m = 1 nA was always applied, and the experiments were systematically repeated in both SA and N_2 (with 50 ppm of residual O_2). Conductance modulation curves were represented in terms of $\{(G/G_0) - 1\}$ to facilitate the comparison of the different recovery transients.
In figure 4a, G_0 of a ZnO nanowire was respectively $G_{0(SA)} = 59 \pm 6$ nS and $G_{0(N2)} = 110 \pm 10$ nS in SA and N_2. UV illumination gave rise to photoresponses 4.2 times higher in N_2 than in SA. Equivalent responses were monitored with the rest of nanowires, confirming that surface interaction mechanisms dominate UV photoresponse and PPC. To decouple bulk and surface phenomena, some of them were passivated with PMMA. Previous works proposed that coating ZnO with polymers not only prevents the interaction of its surface with gases, but it also passivates the electron states of metal oxides associated to dangling bonds located at the surface [19,38-40]. The conductance in darkness of the coated sample ($G_{0(PMMA)} = 1400 \pm 120$ nS) was 24 times higher than in SA ($G_{0(SA)} = 59 \pm 6$ nS), whereas photoresponse was found to increase 12 times in comparison to the response in SA.

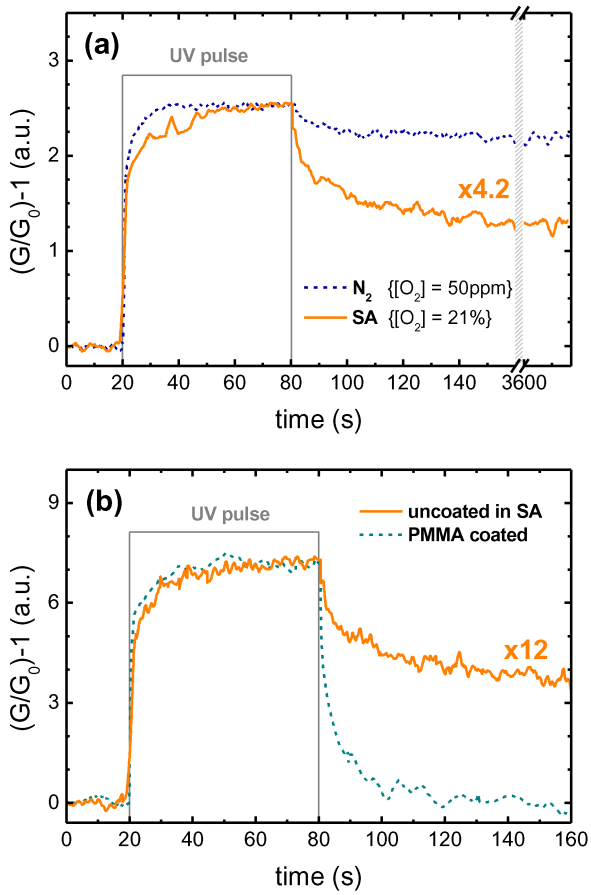

Figure 4. Relative conductance $\{(G/G_0) - 1\}$ of a ZnO nanowire with a 60 s UV pulse (photon flux Φ_{ph} = $3.3 \cdot 10^{18}$ $m^{-2}s^{-1}$, wavelength λ = 340 ± 10nm) acquired at low-probing current conditions (I_m = 1nA). Solid-orange plots were rescaled (multiplying the data by x4.2 and x12, respectively) to ease the comparison of the recovery processes. (a) Two different atmospheres were used: synthetic air (SA) and nitrogen (N_2). The oxygen concentration was $[O_2]_{SA}$ = 210000 ppm and $[O_2]_{N2}$ = 50 ppm, respectively. Response to the UV pulse in N_2 was 4.2 times larger than in SA. (b) Relative conductance $\{(G/G_0) - 1\}$ of a ZnO nanowire with the same UV pulse before and after coating the nanostructure with PMMA. Response to the UV pulse after coating was 12 times larger than before.

3.3.b Modelling PPC in ZnO nanowires

The electrical properties of metal oxide nanowires are strongly influenced by the environment. In general, oxygen molecules in air absorb onto their surface trapping conduction electrons from the bulk [41]. This process leads to the appearance of a negative charge distribution fixed at the surface, which is generally described with an upward band bending [41]. In the steady-state, this phenomenon reduces the effective conduction channel along the nanowires and modulates G as [42,43],

$$G = |e| n_0 m \frac{p\left(r_{NW} - l\right)^2}{L_{NW}} \qquad (2)$$

where G is the conductance of a nanowire of radius r_{NW} and length L_{NW}, e the fundamental charge, n_0 the concentration of free carriers, μ their electrical mobility and λ the width of the depletion layer, which depends on the chemisorbed species.

In oxygen-rich atmospheres, λ grows and thus, lower electrical conductance is observed. On the contrary, thinner λ arises with low pressure oxygen atmospheres and higher conductance values are monitored [42]. This prediction is in agreement with our experimental data:

$$G_{0\,(PMMA)} = 1400\text{nS} \quad >> \quad G_{0\,(N_2)} = 110\text{nS} \quad > \quad G_{0\,(SA)} = 59\text{nS}\,. \qquad (3)$$

The λ size in SA for ZnO nanowires can be estimated by solving the Poisson equation [43],

$$V_b = \frac{|e|n_0}{4\varepsilon_0\varepsilon_r}\left[\left(2r_{NW}^2 - \lambda^2\right) - 2\left(r_{NW} - \lambda\right)^2 \log\left(r_{NW}/(r_{NW} - \lambda)\right)\right]. \qquad (4)$$

For r_{NW} ~ 95nm, λ ≈ 35nm was found considering a typical barrier of V_b ~ 0.55eV [43], n_0 = $4\cdot10^{17}$cm^{-1} [10] (see supporting information), and the relative dielectric constant of ZnO (ε_r = 8.65 [44]). This λ value is also in good correspondence with the literature [43].

In fact, this simple model explains the modulation of G in N_2 and SA (up to a factor 2.5 [45]), but it fails with the huge change observed in PMMA-coated samples (factor 12). In this case, the contribution of the electrical mobility must be taken into account as well, since high mobility values have been reported in coated nanowires due to the reduction of electron scattering at their surfaces [19,38-40]. Following a methodology explained in detail elsewhere [10] (see supporting information), the electrical mobility of both coated and uncoated ZnO nanowires in SA was estimated ($\mu_{(SA)} = 5 \pm 2$ cm^2 V^{-1} s^{-1} and $\mu_{(PMMA)} = 53 \pm 8$ cm^2 V^{-1} s^{-1}). This difference (factor 10) explains the variation of G between the two experiments (see equations (2) and (3)).

Under illumination, UV photons generate electron-hole pairs in the bulk of the nanowires. After a few seconds, photoresponse (ΔG_{ph}) reaches a steady-state in which the recombination and the generation rates equal (figure 5.a and 5.b). Thus, the excess of n and p carriers (Δn and Δp) is given by [46],

$$\Delta G_{ph} \propto \Delta n = \Delta p = g\tau \qquad (5)$$

where g is the photogeneration rate of carriers per volume unit and τ their mean lifetime. If the number of recombination mechanisms is large, τ can be roughly estimated with the help of the Mathiessen's rule [46],

$$\frac{1}{\tau} = \sum_j \frac{1}{\tau_j}\,. \qquad (6)$$

Some authors claim the existence of two different mechanisms which steer the photoresponse in metal oxides [28,29,47]. The former one is a fast band-to-band recombination in their bulk with characteristic times in the nanosecond range (figure 5.a) [13]. The latter, which becomes dominant in nanosized materials [48], is highly dependent on the existence of chemisorbed oxygen molecules at their surfaces, since holes discharge oxygen species from the surface by indirect electron-hole recombination mechanisms (figure 5.a) [47]. Thus, equation (5) can be rewritten as,

$$\Delta G_{ph} \propto \Delta n = \Delta p = \frac{g}{1/\tau_{bulk} + 1/\tau_{surf}} \qquad (7)$$

where τ_{bulk} and τ_{surf} are the lifetime of the photocarriers recombined in the bulk and at the surface. In oxygen-rich environments, surface recombination is favoured and lower ΔG_{ph} are produced. On the contrary, this mechanism is blocked in coated samples, explaining the experimental trend of measured photoresponses (figure 4),

$$\Delta G_{ph\,(PMMA)} \quad > \quad \Delta G_{ph\,(N_2)} \quad > \quad \Delta G_{ph\,(SA)}\,. \qquad (8)$$

When light is switched off, the two recombination mechanisms swiftly contribute to recover the initial carrier concentration in the nanowires. Nevertheless, the built-in potential near the surface caused by oxygen adsorption separates the photogenerated pairs: holes accumulate at the outer shell of the nanowire and electrons remain together in the inner part. This photogenerated effect prevents the recombination of a fraction of the pairs, whereby PPC is observed after the UV pulse (figure 5.c). Thereby $\Delta G/G_0$ will strongly depend on the oxygen content in air. That is to say, the higher this experimental parameter is the more efficient recombination through the surface and the less important the PPC becomes (figure 4.a). In the particular case of PMMA-coated samples, nanowires approaches to the so-called flat-band conditions [49] and thus, no charge separation takes place, favouring a complete recovery of the conductance baseline in dark (figure 4.b).

If temperature increases, carriers gain thermal energy and they can easily overcome the built-in potential. In this case, PPC is not observed (figure 2).

According to first principles calculations, oxygen in air (O_2) undergoes a dissociative chemisorption at the surface oxygen vacant (VO) site in ZnO non-polarsurfaces [50,51], via filling the VO with one O atom originated from the adsorbate. This dissociation of O_2 is exothermic and barrierless, and may even occur spontaneously at room temperature. This result suggests that VO are the surface sites at which oxygen assisted recombination of electrons and holes take place. From the point of view of the electron states, we demonstrated that VO sites are associated to surface states with energy 0.5 eV above the valence band edge [52].

The here-proposed model only assumes the existence of a built-in potential to justify the charge pairs separation and hole accumulation near the surface of the material. Since this feature is common with other metal oxides, the model can be easily extended to other materials with similar PPC effects [53]. This model does not take into account the large number of bulk charge states located within the band gap of ZnO [35] with a strong influence in many applications, like gas sensing [35]. Other simplifications that may limit the model are those related to the flat band approximation in coated samples. These simplifications may prevent the explanation of the few-seconds kinetics to reach the steady state, which is experimentally observed even when the samples are coated with PMMA.

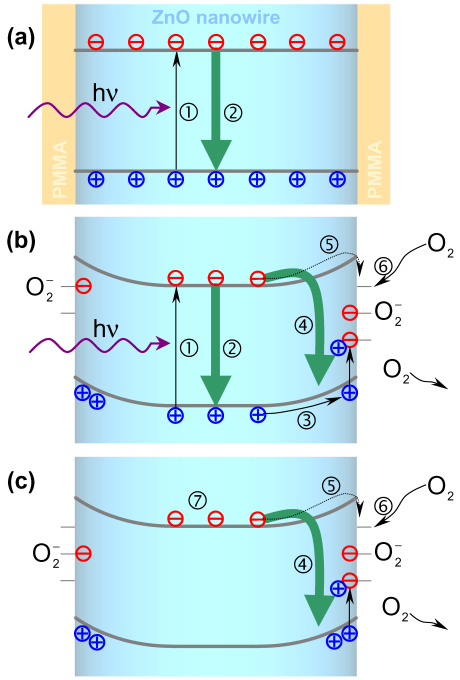

Figure 5. (a) Flat-band situation. When the material is illuminated with above-bandgap photons the ① *photogeneration of electron-hole pairs* equals the ② *band-to-band recombination mechanism* reaching steady conductance values. This case corresponds to the bulk material and also to the nanowires passivated with PMMA. (b) If band-bending near the surface is considered, an additional mechanism appears due to charge separation by this built-in potential: ③ *holes tend to accumulate near the surface* and recombine with electrons in an ④ *oxygen-assisted surface recombination mechanism*. ⑤ *Temperature* and ⑥ *adsorption of oxygen* by electron capture facilitates the access of the electrons to the surface. (c) When illumination is switched off, the bulk-like recombination mechanism rapidly extinguishes holes in the inner part of the nanowire. The remaining unpaired electrons are the responsible of the ⑦ *persistent photoconductivity situation* which can only be reverted by favouring the ④ *oxygen-assisted surface mechanism*.

4. Conclusions

The study of Persistent PhotoConductivity (PPC) in individual ZnO nanowires demonstrated that the electrical transport properties in these nanomaterials are determined by the surface in two different ways. On the one hand, the effective mobility and the available free carriers -μ and n_o- are controlled by the surface recombination mechanisms assisted by the oxidizing molecules in air. On the other hand, the photoconductance G is modified by the changes in the size of the depletion layer -?-.

In particular, PPC essentially depends on the built-in surface potential originated by the surface charges. Under UV illumination, this built-in potential induces electron-hole separation, and hole accumulation at the surface. Once light is switched off, accumulated charges need recombination paths to be drained and PPC appears if these paths are not available.

It is experimentally observed that PPC recovery times are linked with the availability of recombination paths. We observed that PPC was quickly reverted after increasing either the probing current -self-heating by Joule dissipation- or the oxygen content in air -favouring the surface recombination mechanisms. These experimental results and the proposed model helped us to elucidate the origin of the PPC in nanostructures. Thus, PPC can be completely blocked by heating the final devices or passivating their surfaces. It is noteworthy that PMMA coatings totally blocked PPC, overcoming one of the main limitations to integrate ZnO and other metal oxides in a new generation of optoelectronic nanodevices.

Acknowledgments

This work has been partially supported by the Spanish Ministry of Education and Science (MEC) through the projects n–MOSEN (MAT2007-66741-C02-01) and MAGASENS (NAN2004-09380-C04-01), and the UE and NanoSciEra Consortium through the project NAWACS (NAN2006-28568-E). JDP and RJD are indebted to the MEC for the FPU grant.

References

[1] Fan H J, Werner P and Zacharias M 2006 *Small* **2** 700-17
[2] Law M, Goldberger J and Yang P 2004 *Annu. Rev. Mater. Res.* **34** 83-122
[3] Wang Z L 2004 *J. Phys.: Condens. Matter.* **16** R829-58
[4] (a) Mathur S, Barth S, Shen H, Pyun J-C and Werner U 2005 *Small* **1** 713-17 (b) Mathur S and Barth S 2007 *Small* **3** 2070-5
[5] Chang P-C, Chien C-J, Stichtenoth D, Ronning C and Lu J G 2007 *Appl. Phys. Lett.* **90** 113101
[6] Lieber C M and Wang Z L 2007 *MRS Bull.* **32** 99-104
[7] Patolsky F, Timko B P, Zheng G and Lieber C M 2007 *MRS Bull.* **32** 142-9
[8] Yang M-R, Chu S-Y and Chang R-C. 2007 *Sens. Actuators B* **122** 269-73.
[9] Hernandez-Ramirez F, Tarancon A, Casals O, Rodriguez J, Romano-Rodriguez A, Morante J R, Barth S, Mathur S, Choi T Y, Poulikakos D, Callegari V and Nellen P M 2006 *Nanotechnol.* **17** 5577-83
[10] Hernandez-Ramirez F, Tarancon A, Casals O, Pellicer E, Rodriguez J, Romano-Rodriguez A, Morante J R, Barth S and Mathur S 2007 *Phys. Rev. B* **76** 085429
[11] Law M, Kind H, Messer B, Kim F and Yang P D 2002 *Angew. Chem. Int. Ed.* **41** 2405-8
[12] Heo Y W, Norton D P, Tien L C, Kwon Y, Kang B S, Ren F, Pearton S J and LaRoche J R 2004 *Mater. Sci. Eng. R* **47** 1-47.
[13] Wang J X, Sun X W, Wei A, Lei Y, Cai X P, Li C M, Dong Z L 2006 *Appl. Phys. Lett.* **88** 233106
[14] Wang Z L and Song J H 2006 *Science* **312** 242-6
[15] Kind H, Yan H, Messer B, Law M and Yang P 2002 *Adv. Mater.* **14** 158-60
[16] Fan Z Y, Chang P C, Lu J G, Walter E C, Penner R M, Lin C H and Lee H P 2004 *Appl. Phys. Lett.* **85** 6128-30
[17] Law J B K and Thong J T L 2006 *Appl. Phys. Lett.* **88** 133114

[18] Soci C, Zhang A, Xiang B, Dayeh S A, Aplin D P R, Park J, Bao X Y, Lo Y H and Wang D 2007 *Nano Lett.* **7** 1003-9
[19] Prades J D, Jimenez-Diaz R, Hernandez-Ramirez F, Fernandez-Romero L, Andreu T, Cirera A, Romano-Rodriguez A, Cornet A, Morante J R, Barth S and Mathur S 2008 *J. Phys. Chem. C* Article in press.
[20] Liu Y, Gorla C R, Liang S, Emanetoglu N, Lu Y, Shen H and Wraback M J 2000 *J. Electron. Mater.* **29** 69-74
[21] Lany S and Zunger A 2005 *Phys. Rev. B* **72** 035215
[22] Janotti A and Van de Walle C G 2005 *Appl. Phys. Lett.* **87** 122102
[23] Nayak J, Kasuya J, Watanabe A and Nozaki S 2008 *J. Phys.: Condens. Matter* **20** 195222
[24] Melnick D A 1957 *J. Chem. Phys.* **26** 1136-46
[25] Sheinkman M K and Shik A Y 1976 Sov. Phys.-Semicond. 10 128-48
[26] Studenikin S A, Golego N and Cocivera M 2000 *J. Appl. Phys.* **87** 2413-21
[27] Sharma P, Sreenivas K and Rao K V 2003 *J. Appl. Phys.* **93** 3963-70
[28] Li Q H, Gao T, Wang Y G and Wang T H 2006 *Appl. Phys. Lett.* **86** 123117
[29] Reemts J and Kittel A 2007 *J. Appl. Phys.* **101** 013709
[30] Claflin B, Look D C and Norton D R 2007 *J. Elect. Mater.* **36** 442-5
[31] ZnO nanowires were synthesized with a commercial Atomate's CVD system. The source material was 1:1 molar mixture of ZnO (metal basis 99.99 %) and graphite powder provided by Alfa Aesar. Crystalline nanowires with average radii $\langle r_{NW} \rangle = 90 + 15$ nm and lengths up to L = 30 were obtained [3]. High resolution TEM images showed well-faceted single crystalline nanowires with dislocation free bodies grown along the [0001] direction (see supporting information).
[32] Hernandez-Ramirez F, Rodriguez J, Casals O, Russinyol E, Vila A, Romano-Rodriguez A, Morante J R and Abid M 2006 *Sens. Actuators, B* **118** 198-203
[33] Seoul Optodevices model T9F34C
[34] Hernandez-Ramirez F, Prades J D, Tarancon A, Barth S, Casals O, Jiménez-Diaz R, Pellicer E, Rodriguez J, Juli M A, Romano-Rodriguez A, Morante J R, Mathur S, Helwig A, Spannhake J and Mueller G 2007 *Nanotechnol.* **18** 495501
[35] Özgür Ü, Alivov Ya I, Liu C, Teke A, Reshchikov M A, Dogan S, Avrutin V, Cho S-J and Morkoç H 2005 *J. Appl. Phys.* **98** 041301
[36] Look D C 1983 *Semicond. Semimet.* **19** 75-170
[37] Prades J D, Jimenez-Diaz R, Hernandez-Ramirez F, Barth S, Cirera A, Romano-Rodriguez A, Mathur S and Morante J R 2008 *Appl. Phys. Lett.* Submitted.
[38] Park W I, Kim J S, Yi G-C, Bae M H and Lee H J 2004 *Appl. Phys. Lett.* **85** 5052-4
[39] He J H, Lin Y H, McConney M E, Tsukruk V V, Wang Z L and Bao G 2007 *J. Appl. Phys.* **102** 084303-4
[40] (a) Hong W K, Sohn J I, Hwang, Kwon S-S, Jo G, Song S, Kim S-M, Ko H-J, Park S-J, Welland M E and Lee T 2008 *Nano Lett.* **8** 950-6 (b) Hong W K, Kim B-J, Kim T-W, Jo G, Song S, Kwon S-S, Yoon A, Stach E A and Lee T, 2008 *Colloids Surf. A: Physicochem. Eng. Aspects* **313–314** 378–82
[41] Arnold M S, Avouris P, Pan Z W and Wang Z L 2003 *J. Phys. Chem. B* **107** 659-63
[42] Hernandez-Ramirez F, Prades J D, Tarancon A, Barth S, Casals O, Jimenez-Diaz R, Pellicer E, Rodriguez J, Morante J R, Juli M A, Mathur S and Romano-Rodriguez A 2008 *Adv. Func. Mater.* Article in press. DOI: 10.1002/adfm.200701191
[43] Comini E, Guidi V, Malagu C, Martinelli G, Pan Z, Sberveglieri G and Wang Z L 2004 *J. Phys Chem* **108** 1882-87
[44] Bhargava B 1997 *Properties of Wide Bandgap II–VI Semiconductors* (London: Inspec)
[45] According to equation (2), the maximum conductance (G_{MAX}) of the nanowire corresponds to the case of null depleted layer ($\lambda = 0$). The formation of a depleted layer of thichness λ results in a decrease of the conductivity (G_{min}). The change in the conductivity due to the formation of this depleted layer is thus $G_{MAX}/G_{min} = (r_{NW})^2 / (r_{NW} - \lambda)^2$. In our case, $r_{NW} = 95$nm, $\lambda = 35$nm and $G_{MAX}/G_{min} = 2.5$.
[46] Sze S M 1981 *Physics of Semiconductor Devices* (New York: John Wiley & Sons, Inc)

[47] Lin Y, Wang D, Zhao Q, Li Z, Ma Y and Yang M 2006 *Nanotechnol.* **17** 2110-5
[48] The contribution of surface mechanisms is especially important in the case of nanowires because their diameters are significantly lower than the diffusion length of carriers in ZnO ($L_{ZnO} \sim 1\mu m$) [35].
[49] Surface passivation implies that there are not any gas molecules chemisorbed onto the ZnO surface [19,38-40]. In this situation, no charge is trapped at the nanowire' surface and no band-bending occurs. This obviously is a drastic approximation.
[50] An W, Wu X and Zeng X C 2008 *J. Phys. Chem. C* **112** 5747-55
[51] Yan Y and Al-Jassim M M 2005 *Phys. Rev. B* **72** 235406
[52] Prades J D, Cirera A, Morante J R and Cornet A 2007 *Thin Sol. Films* **515** 8670-3
[53] Geraldo V, Scalvi L V A, Morais E A, Santilli C V, Miranda P B and Pereira T J 2005 *J. European Ceramic Soc.* **25**, 2825-28

A. Supporting information

A.1 Synthesis, morphology and structure of the ZnO nanowires

ZnO nanowires were fabricated via a vapor-phase carbothermal transport process inside an Atomate's chemical vapour deposition (CVD) system. The source material was a 1:1 molar mixture of commercial ZnO (metal basis, 99.99%) and graphite powder (crystalline, 300 mesh, 99%) from Alfa Aesar. Gold nanoparticles were used as catalytic islands on amorphous alumina substrates. Uniform and crystalline nanowires were obtained with mean radius $\langle r_{NW} \rangle$ = 90±15 nm and lengths up to L = 30 μm (Figure I). High resolution TEM images showed well-faceted single crystalline nanowires with dislocation free bodies grown along the [0001] direction (Figure II).

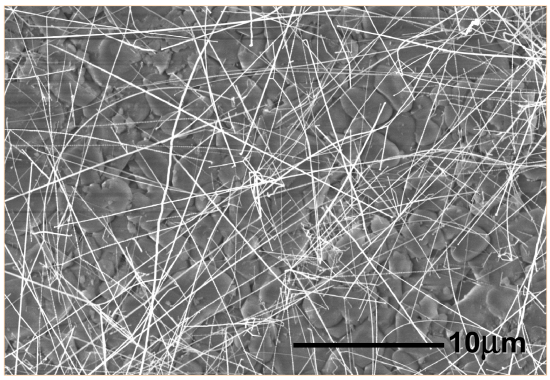

Figure I. SEM micrograph of the as grown ZnO nanowires. Nanostructures with mean radius r_{NW} = 90±15 nm and lengths up to 30 μm were obtained.

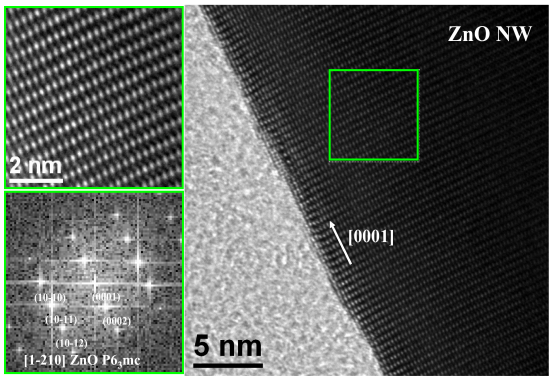

Figure II. HRTEM analysis of a ZnO nanowire. Crystalline and dislocation-free ZnO grow along the [0001] direction. Surface roughness is less than 3 monolayers. *Thanks are due to Dr. J. Arbiol.*

A.2 Electrical I(V) characteristics

The nanowires' I(V) characteristics measured in 2 and 4–probe configurations are shown in figure III. In the 2–probe case, we observed a symmetric non-linear characteristic corresponding to two back-to-back Schottky diodes in series with the resistance of the nanowire (1/G). The conduction through the metal-semiconductor (Pt/ZnO) junction is properly described by thermoionic emission and interface states assisted tunnelling (TE+TuSA) [a,b]. According to this model, the voltage drop across the hole structure in 2–probe configuration ($V_{(2\text{-}p)}$) is [a,b]

$$V_{(2-p)} = V_{diode} + V_{NW} = \left(\frac{\ln I - \beta}{\alpha(n)} \right)^4 + \frac{I}{G(n,\mu)} \qquad \text{(i)}$$

where I is the current, G is the conductance of the nanowire and α and β are parameters of the TE+TuSA model for the voltage drop at the reverse biased diode (V_{diode}). It is noteworthy that α and G are analytic functions dependent on the free carriers concentration n and the mobility μ. Thus, fitting the experimental curve to equation (i) it is possible to estimate G and also decouple n and μ. A detailed explanation of this procedure can be found elsewhere [a]. In dark ($_0$) and synthetic air (SA), the conductance of our nanowires was $G_{0(SA)}$ = 60 ± 8 nS and the correspondent carrier concentration and mobility were $\mu_{(SA)}$ = 5 ± 2 $cm^2\ V^{-1}\ s^{-1}$ and $n_0 = 4 \cdot 10^{17}\ cm^{-1}$.

In the case of 4-probe measurements, we observed a linear characteristic only due to the resistance of the nanowire. From the slope of this plot we estimated the conductance in dark of the nanowire in $G_{0(SA)}$ = 59±6 nS which was in accordance with the previous estimation. The measurements reported in the main text were performed in 4-probe configuration to avoid the interfering effect form the contacts.

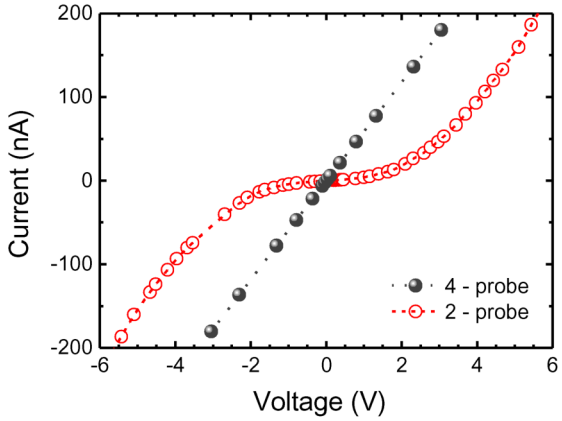

Figure III. I(V) characteristics of a single ZnO nanowire acquired in 2 and 4-probe configurations in dark conditions. Lines represent the mathematical fitting to estimate the values described in the text.

A.3 Wavelength photoresponse threshold in ZnO nanowires

To stimulate the photoresponse in ZnO nanowires, we used a set of LEDs [c] of energies hν above and below the bandgap of this semiconductor (E_{gap}(ZnO) = 3.37eV [d]). In figure IV we show the fully-ohmic I(V) characteristics under illumination at different energies. For hν below the E_{gap}(ZnO), photocurrent increase in less than 5%, while for hν above E_{gap}(ZnO), the photoresponse is about 160%. This indicates that photoconduction is essentially due to band-to-band electron-hole pairs generations. From the technological point of view, this results also suggest that ZnO nanowires are almost visible-blind UV photodetectors with flat response in the near-UV region. For this reason, we centre our study in the source at hν = 3.64eV (340nm).

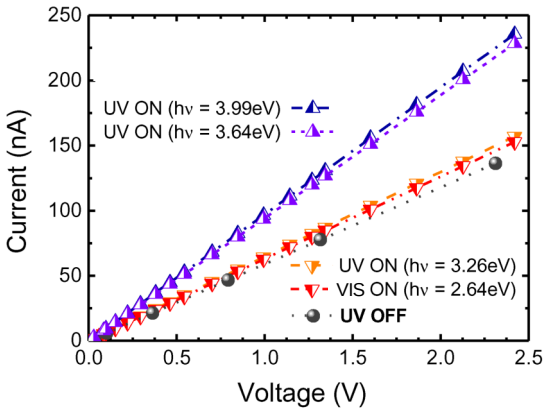

Figure IV. 4-probe I(V) characteristics of a single ZnO nanowire at different illumination conditions. Significant photoresponse is only obtained with photon energies above E_{gap}(ZnO) = 3.36eV. All measurements were acquired under photon flux $\Phi_{ph} = 3.3 \cdot 10^{18}$ $m^{-2}s^{-1}$.

A.4 UV transmittance and conductance of PMMA layers

To evaluate the transparency of PMMA to UV light, transmittance spectroscopy experiments were performed on PMMA layers of thickness (475 ± 50) nm deposited over fused silica substrates (figure V). In figure VI, the transmittance spectrum of one of these layers is shown, after subtracting the silica contribution. Transmittances values above 90% were obtained for wavelengths from 250 nm to 800 nm.

Chips with pre-patterned microelectrodes were also coated in order to estimate the conductance and photoresponse of these PMMA layers. Typical conductance values were always below 0.1 nS, and any significant change was observed after UV illumination (figure VII).

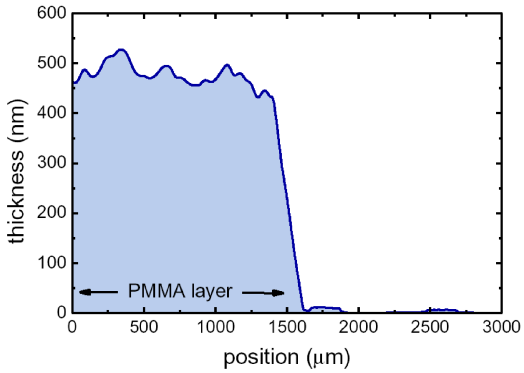

Figure V. Perfilometry profile of a cracked layer of PMMA deposited onto a silica substrate.

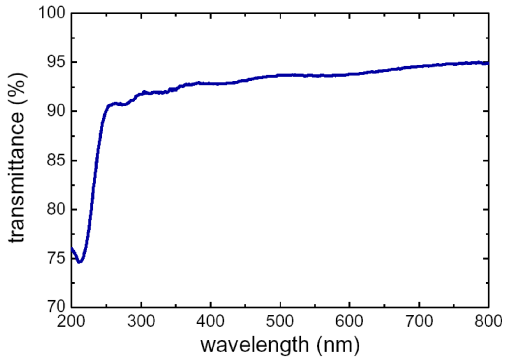

Figure VI. Transmittance spectrum of a PMMA layer. Contribution from the silica substrate was corrected.

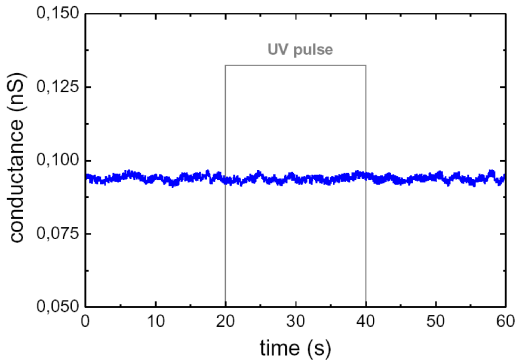

Figure VII. 4-probe measurement of the conductance of a PMMA layer. No response to UV light was observed.

A.4 References:

[a] Hernandez-Ramirez F, Tarancon A, Casals O, Pellicer E, Rodriguez J, Romano-Rodriguez A, Morante J R, Barth S and Mathur S 2007 *Phys. Rev. B* **76** 085429
[b] Zhang Z, Yao K, Liu Y, Jin C, Liang X, Chen Q, Peng L-M 2007 *Adv. Func. Mater.* **17** 2478-89
[c] We used the following light emitting diodes from Seoul Optodevices: T9F31C (310±10nm), T9F34C (310±10nm), UVLED380-10 (380±15nm) and L5T15B (470±5nm).
[d] Özgür Ü, Alivov Ya I, Liu C, Teke A, Reshchikov M A, Dogan S, Avrutin V, Cho S-J and Morkoç H 2005 *J. Appl. Phys.* **98** 041301